Article:
Kameda, M, Bauer, GEW and Barker, J orcid.org/0000-0003-4843-5516 (2022) Magnon spectrum of the amorphous ferromagnet Co4P from atomistic spin dynamics. Physical Review B, 106 (6). L060403. ISSN 2469-9950

https://doi.org/10.1103/physrevb.106.l060403

Magnon spectrum of the amorphous ferromagnet Co_4P from atomistic spin dynamics

Mai Kameda,[1,2] Gerrit E. W. Bauer,[1,3,4,5] and Joseph Barker[1,6,7]

[1]*Institute for Materials Research, Tohoku University, Sendai 980-8577, Japan*
[2]*Department of Applied Physics, Nagoya University, Nagoya 464-8603, Japan*
[3]*WPI Advanced Institute for Materials Research, Tohoku University, Sendai 980-8577, Japan*
[4]*Zernike Institute for Advanced Materials, University of Groningen, 9747 AG Groningen, The Netherlands*
[5]*Kavli Institute for Theoretical Sciences, University of Chinese Academy of Sciences (UCAS), Beijing 100190, China*
[6]*School of Physics and Astronomy, University of Leeds, Leeds LS2 9JT, United Kingdom*
[7]*Bragg Centre for Materials Research, University of Leeds, Leeds LS2 9JT, United Kingdom*

(Dated: August 12, 2022)

The gapped local minimum in the magnon dispersion, located at a finite wavenumber and frequency, has been observed in the amorphous ferromagnet Co_4P. The feature is called a 'roton-like' excitation and has eluded explanation for decades. We overcome the limitations of previous theories by combining the reverse Monte Carlo method, to determine the atomic structure, with large-scale atomistic spin simulations. This method enables us to include atomic order and spin correlations on an equal footing. We find the roton-like feature is actually gapless, in contrast to the gapped structure found in previous studies. The gapless feature is attributed to amorphous umklapp scattering caused by residual structural order.

Introduction. – Amorphous magnets are technologically important due to their highly tuneable coercivity and magnetisation for, e.g., power transformers and magnetic memories. Commonly used materials include random rare-earth–transition metal alloys such as GdFeCo for magnetooptical devices [1] and CoFe alloys for spintronic devices [2, 3]. The phenomenology of these materials is often not much different from ordered materials, displaying conventional ferro or ferrimagnetic order. On the other hand, in thermally induced switching [4] or long-range magnon transport [5, 6] the local atomic arrangement appears to be important. Magnon transport in amorphous systems is currently a topic of debate since experimental results contradict each other [7, 8]. With the current interest in heat and spin currents in amorphous magnets, we re-investigate the magnon dispersion.

We select Co_4P, a typical amorphous ferromagnet, in this work as a relatively simple representative for amorphous magnets [9]. In the 1970's, Co_4P attracted much interest [9–11], because neutron scattering experiments discovered a local minimum in its magnon dispersion at a finite wavenumber [12]. The feature is reminiscent of the dip in the phonon dispersion of liquid He caused by the "roton" excitation that limits superfluidity [13, 14]. While the similarity of the dispersion relations intrigued researchers, the physical origin remained a mystery. Truly roton-like excitations in other magnetic systems, such as triangular lattice antiferromagnets [15–19] are not applicable for ferromagnets. In concordance with the previous studies, we nevertheless refer to the dip feature as a 'roton-like' excitation even though we arrive at a very different explanation.

We may analyse the magnon dispersion in the quasi-crystalline approximation (QCA) [11, 20] of the amorphous atomic structure, in terms of an isotropic atomic pair-correlation function $g(r)$, with r being the atomic distance. The energy ε of a spin wave with wavenumber Q then reads

$$\varepsilon_{\mathrm{QCA}}(Q) = 4\pi\mu\rho_{\mathrm{m}} \int J(r_{ij}) g(r_{ij}) \left(1 - \frac{\sin Q r_{ij}}{Q r_{ij}}\right) r_{ij}^2 dr_{ij}, \tag{1}$$

where μ is a local moment, ρ_{m} is mean density of the magnetic atoms, $J(r_{ij})$ is the exchange interaction dependent on distance $r_{ij} = |\mathbf{r}_j - \mathbf{r}_i|$, where $\mathbf{r}_i$ ($\mathbf{r}_j$) denotes the position of the i-th (j-th) magnetic atom. With physically motivated models for $J(r_{ij})$ and $g(r_{ij})$, the QCA predicts spectra including a shallow dip close to the wavenumber at which the roton-like feature was observed. Calculations in the effective medium approximation (EMA) that includes spatial correlations to a higher order than the QCA find a deeper valley [21–23]. However, the EMA also proceeds from an isotropic atomic correlation function and the predicted gap is still larger than observed. Shallow dips [24] were also found in numerical simulations based on linear spin wave theory, which approximates spin correlations, for anisotropic atomic correlation functions of hard sphere packing models [25–28]. In essence, all previous approaches have either significantly approximated spatial or spin correlations (or both). On the other hand, Shirane et al. pointed out the difficulties of measuring small gaps by inelastic neutron scattering due to its finite resolution [29]. They already suggested that the roton-like dip might be gapless and possibly caused by umklapp scattering.

In this paper, we report results of extensive atomistic simulations in which both atomic and spin correlations are treated on an equal footing. This enables us to clarify whether the gap is real and the nature of the local dip. This paves the way to study the magnonic transport in amorphous magnets and related spintronic applications [5–8].

Our simulations expose a magnon dispersion that is an intriguing mix of features from the QCA and residual order in an amorphous structure. We find a gapless mirror image of the magnons at $Q = 0$ with parabolic dispersion, centred at the wavenumber at which the static structure factors peak [29] and interpret it as residual umklapp scattering.

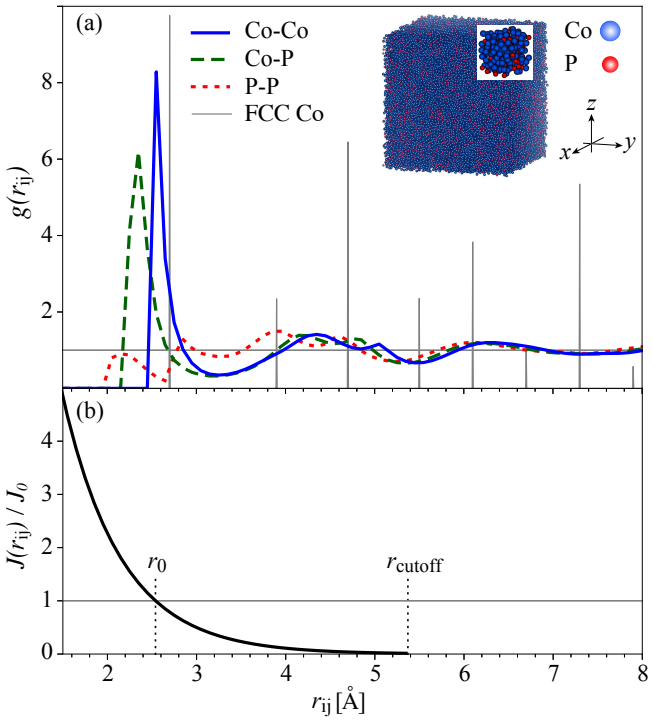

FIG. 1. (a) Correlation functions $g(r_{ij})$ for Co-Co, Co-P, and P-P pairs in Co_4P, obtained as an average over 10 independent configurations generated by RMC. The vertical lines illustrate the δ-function correlations in a FCC crystal with the same volume. The inset shows an example of an RMC generated amorphous Co_4P with 62500 atoms (blue = Co and red = P). (b) Single-exponential exchange interaction $J(r_{ij})$ used in the atomistic spin simulations, which we set to zero for $r_{ij} > r_{\rm cutoff} = 5.45$ Å.

Methods. – The atomic positions in amorphous alloys are not precisely known, but they are not distributed completely randomly either. Our task is to find statistical ensembles that on average describe the specific material properties. The observed roton-like gap depends sensitively on, for example, the alloy composition [12, 30], so it may have a structural origin. Here we generate the amorphous atomic positions by the reverse Monte Carlo (RMC) method [31] under constraints of established observations, which should produce a more realistic model than building an alloy by random packing [25–28].

We use the RMC++ code [32], to generate atomic configurations that reproduce X-ray, neutron and polarised neutron diffraction data for Co_4P [33]. We start with an FCC lattice with substitutional disorder in the form of randomly distributed Co and P in a 4:1 ratio. In each iteration step (a) two atoms can be swapped or (b) a single atom can be moved a small distance in a random direction [32]. Periodic boundary conditions keep the volume constant. The mean-square cost function for a scattering function (i =X-ray, neutron, polarised neutron) reads $\chi_i^2 = \sum_Q^{n_Q} \left(\mathcal{S}_i^{\rm calc}(Q) - \mathcal{S}_i^{\rm exp}(Q)\right)^2 / (n_Q \sigma_i^2)$, where n_Q is number of data points [34], σ_i is a weight that reflects the confidence level of a data set, $\mathcal{S}_i^{\rm calc}(Q)$ and $\mathcal{S}_i^{\rm exp}(Q)$ are the calculated and measured scattering functions for Q. We note that the scattering functions are represented as $\mathcal{S}_i^{\rm calc}(Q) \propto \sum_{mn} \rho_n \int 4\pi r_{ij}^2 dr_{ij} (g_{mn}(r_{ij}) - 1) \sin(Qr_{ij})/(Qr_{ij})$ [35], where $g_{mn}(r_{ij}) = n_{mn}(r_{ij})/(4\pi r_{ij}^2 \Delta r_{ij} \rho_n)$, n_{mn} is the number of neighbours of atom type n at distance from r_{ij} to $r_{ij} + \Delta r_{ij}$ from an atom of type m, Δr_{ij} is a binning width of the histogram, and ρ_n is the number density of type n. Each move that lowers the total cost function $\chi^2 = \sum_i \chi_i^2$ is accepted unconditionally while those that increase χ^2 are accepted with a probability $\exp(\chi^2_{\rm old} - \chi^2_{\rm new})$, where $\chi^2_{\rm old}$ and $\chi^2_{\rm new}$ are the cost function values before and after the move.

We model the atoms by hard spheres with radii $r_{\rm Co} = 1.25$ Å and $r_{\rm P} = 1.00$ Å, ignoring the chemical bonding. We implement the known feature of amorphous compounds like Co_4P that the anions (P in this case) almost never touch [33] by an increased cost when P atoms are closer than 2.75 Å. The stopping criteria of the RMC procedure is $|\chi^2_{\rm old} - \chi^2_{\rm new}|/\chi^2_{\rm new} < 0.8\%$, while the weighted R-factors $R_{w,i}$ [35] or quality of the fits are 25.3%, 28.47%, and 20.5% for i = X-ray, neutron, and polarised neutron. σ_i are respectively $\sigma_{\rm X-ray} = 0.005$, $\sigma_{\rm neutron} = 0.01$, and $\sigma_{\rm polarised} = 0.01$. Further technical details and data files are available in the supplementary information [36].

After the Monte-Carlo iterations converged, as shown in Fig. 1(a), we compute the magnetic properties by atomistic spin dynamics (ASD) [37–39]. The i-th Co atom at $\mathbf{r}_i$ has a local moment $\mu = \mu_{\rm B}$ (Bohr magneton) [12] and direction $\mathbf{S}(\mathbf{r}_i)$ with $|\mathbf{S}| = 1$. The non-magnetic P atoms are treated as vacancies [40]. Assuming that anisotropies and superexchange interactions average out in random alloys, we adopt the isotropic Heisenberg model Hamiltonian,

$$\mathscr{H} = -\tfrac{1}{2} \sum_{i \neq j} J(r_{ij}) \mathbf{S}(\mathbf{r}_i) \cdot \mathbf{S}(\mathbf{r}_j) - \mu \mathbf{B} \cdot \sum_i \mathbf{S}(\mathbf{r}_i), \quad (2)$$

where $\mathbf{B}$ is an external magnetic field. $J(r_{ij})$ extends beyond nearest neighbours. Our knowledge of the exact functional form of $J(r_{ij})$ has not progressed much in the past decades, so we implemented several options, such as a step function, exponential decay, and oscillating (RKKY) functions [11] and with different ranges. Since the results do not change significantly, we concluded that precise distance dependence is not an important issue. In the following, we use the exponential decay shown in Fig. 1(b),

$$J(r_{ij}) = J_0 \exp\left(-\frac{r_{ij} - r_0}{w}\right) \text{ for } r_{ij} < r_{\rm cutoff}, \quad (3)$$

where $J_0 = 6.733$ meV, $r_0 = 2.54$ Å, and a decay length $w = 0.66$ Å. $r_{\rm cutoff} = 5.45$ Å is a cutoff radius above which we set $J(r_{ij}) = 0$. Truncating the interaction at large distances does not affect the results, but reduces the computational cost. With these values the curvature of the magnon dispersion $\epsilon(Q)$ corresponds to the experimental spin wave stiffness of amorphous Co_4P, $D = \frac{1}{2}[\partial^2 \epsilon(Q)/\partial Q^2]_{Q=0} = 135$ meVÅ^2 [11]. In order to emphasise the effects of the disorder, we compare results

for amorphous Co_4P with those for hypothetical crystalline FCC Co with the same volume and parameters.

The Landau-Lifshitz equation for a local moment reads

$$\frac{d\mathbf{S}(\mathbf{r}_i)}{dt} = -\gamma\left[\mathbf{S}(\mathbf{r}_i)\times\mathbf{H}(\mathbf{r}_i) + \alpha\mathbf{S}(\mathbf{r}_i)\times(\mathbf{S}(\mathbf{r}_i)\times\mathbf{H}(\mathbf{r}_i))\right], \tag{4}$$

where t is time, $\gamma = 1.76\times10^{11}$ rad s^{-1}T^{-1} is the gyromagnetic ratio, $\alpha = 0.01$ is a damping constant, and $\mathbf{H}(\mathbf{r}_i) = \boldsymbol{\xi}(\mathbf{r}_i) - (1/\mu)(\partial\mathscr{H}/\partial\mathbf{S}(\mathbf{r}_i))$ is the effective magnetic field on the spin at $\mathbf{r}_i$. $\boldsymbol{\xi}(\mathbf{r}_i)$ is a fluctuating field that provides a temperature to the spin system. We use a quantum thermostat that obeys the fluctuation-dissipation theorem [41],

$$\langle\xi_a(\mathbf{r}_i,t)\rangle = 0;\ \langle\xi_a(\mathbf{r}_i)\xi_b(\mathbf{r}_j)\rangle_\omega = \delta_{ij}\delta_{ab}\frac{2\alpha}{\gamma\mu\beta}\frac{\hbar\omega}{e^{\beta\hbar\omega}-1}, \tag{5}$$

where a and b are Cartesian components, ω is the frequency, $\beta = (k_BT)^{-1}$ is the inverse thermal energy with k_B is the Boltzmann constant and T is temperature, $\hbar$ is Dirac's constant, $\langle\cdots\rangle$ is a statistical time average, and $\langle\cdots\rangle_\omega$ is a statistical average in frequency space. This thermostat describes thermodynamic properties well up to the Curie temperature [42, 43]. Details of the numerical implementation of the ASD method are available in the supplementary information [36]. Our combination of RMC for the atomic structure, the ASD with the quantum thermostat, and the raw computational power to handle large systems all drastically improve previous approaches to simulate random magnets [20–22, 24].

Our algorithm first equilibrates a large number of spins (62500) to a constant temperature. We then carry out the thermodynamic averaging of the desired properties by collecting fluctuating spin trajectories around their equilibrium values up to 0.4 ns. Even though the systems size is already large, we confirm ergodicity by averaging over 10 realisations of the amorphous arrangement of atoms.

Results. – Fig. 1(a) shows the calculated pair-correlation functions $g(r_{ij})$ of Co-Co, Co-P, and P-P pairs in amorphous Co_4P and Co-Co pairs in crystalline FCC. g_{PP} is featureless with a weak maximum at $\sim$ 4 Å, so P is nearly homogeneously distributed and only few P atoms touch each other, as intended by the extra cost for their proximity. The observed double peaked behaviour in g_{CoCo} around 4.4 Å and 5.0 Å indicates short-range order, a common feature of amorphous metalloids [11]. The average number of nearest neighbours, counted as atoms within a radius r_{nbr}, is 7.53 for Co-Co ($r_{nbr} = 3.1$ Å), 1.96 for Co-P ($r_{nbr} = 3.0$ Å), and 0.30 for P-P ($r_{nbr} = 2.75$ Å), where r_{nbr} has been chosen based on the first peak of the $g(r_{ij})$ for each pair. We show an example of an RMC generated atomic configuration in the inset to Fig 1(a).

The excellent agreement of the scattering functions generated by the optimised structures and those inferred from the experiment [33], shown in Fig. 2(a)–(c), demonstrates the validity of the RMC procedure [36].

Fig. 3(a) shows the temperature dependence of the dimensionless magnetisation $\mathbf{M}(T) = \langle(1/N)\sum_{i=1}^{N}\mathbf{S}(\mathbf{r}_i)\rangle_T$,

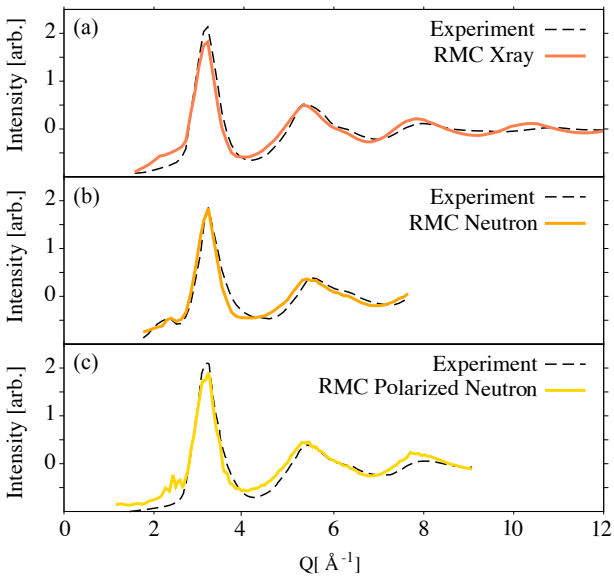

FIG. 2. (a) X-ray, (b) neutron, and (c) polarized neutron scattering functions of Co_4P. The solid lines are an average of 10 independent configurations generated by our RMC method [36]. The dashed lines are the experimental results [33].

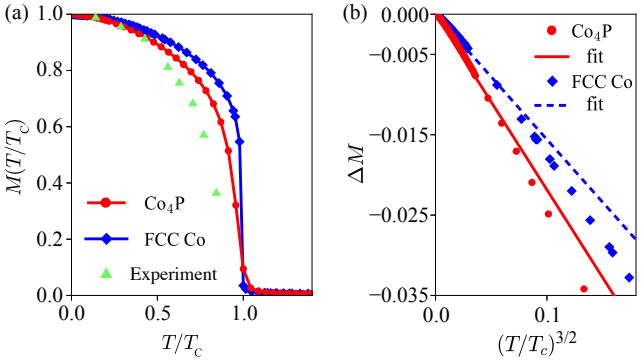

FIG. 3. (a) Temperature dependence of the magnetisation $M(T/T_C)$ of amorphous Co_4P (circle) and hypothetical crystalline FCC Co (diamond). Curie temperatures are $T_C \sim 500$ K for both systems. Green triangles are experimental results [44]. (b) Normalised temperature $(T/T_C)^{3/2}$ vs. reduced magnetisation $\Delta M = M(T/T_C) - 1$. Solid and dashed lines are low-temperature fits to Bloch's law $\Delta M = -B_{3/2}(T/T_C)^{3/2}$.

where N is total number of magnetic atoms, for the amorphous and crystalline systems and experimental data for amorphous Co_4P [44]. The crystalline system has a larger lattice constant than the physical FCC Co, which is a good metal with s-d hybridised bands and high Curie temperature T_C. The susceptibilities (not shown) of both the hypothetical FCC Co and Co_4P peak at $T_C \sim 500$ K. The experimental T_C of Co_4P, 620–720K [12, 45], is higher than calculated but we reproduce the experimental spin wave stiffness and low temperature behavior well. At low temperatures ($T \ll T_C$) the magnetisation of both crystalline and amorphous systems de-

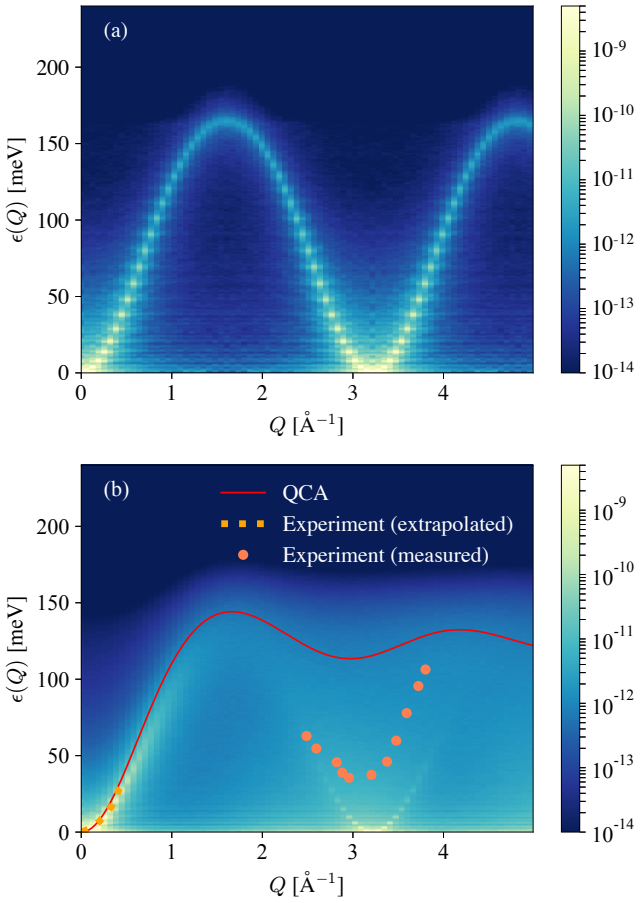

FIG. 4. (a)-(b) Calculated inelastic neutron scattering cross section Eq. (6) of (hypothetical) crystalline FCC Co (a) and Co_4P and the QCA analytic prediction (red solid line) (b) at temperature $T = 300\,\mathrm{K}$. In panel (b), the magnon (dashed orange line) and roton-like excitations (orange dots) [12] observed at room temperature are overlaid for comparison.

crease according to Bloch's law $M(T) = 1 - B_{3/2}(T/T_C)^{3/2}$, with $B_{3/2}$ being the coefficient, as shown in Fig. 3(b). We find $B_{3/2} = 0.16$ for the FCC Co, which is very close to the experimental value of $B_{3/2} = 0.17$ for FCC lattices [11]. The larger $B_{3/2} = 0.22$ for amorphous Co_4P reflects a reduced spin wave stiffness [11]. However, it is about a half the reported $B_{3/2} \sim 0.45$ inferred from magnetometry measurements [45]. These discrepancies of T_C and $B_{3/2}$ might be due to non-collinearities in the magnetic ground state caused by the superexchange via P or local anisotropies [46]. Moreover, the value of $B_{3/2}$ inferred from experimental neutron scattering measurements of the stiffness has generally been smaller than that from magnetometry for a variety of amorphous ferromagnets [46–48]. It is a large parameter space to explore and we do not pursue the issue in more detail here.

Next, we address the unusual roton-like dip observed in the inelastic neutron scattering spectra of Co_4P. To this end, we compute the inelastic neutron scattering cross section for a single magnetic species [49],

$$\mathcal{S}(\mathbf{Q},\omega) = \frac{g_n^2 r_c^2}{2\pi\hbar} f^2(Q) \sum_{ab} \left(\delta_{ab} - \hat{Q}_a \hat{Q}_b\right) \sum_{i,j} e^{-i\mathbf{Q}\cdot\mathbf{r}_{ij}} \times \int_{-\infty}^{\infty} e^{-i\omega t} \left[\langle S_a(\mathbf{r}_i,0) S_b(\mathbf{r}_j,t)\rangle - \langle S_a(\mathbf{r}_i)\rangle \langle S_b(\mathbf{r}_j)\rangle\right] dt, \tag{6}$$

where $g_n = 1.931$ is the neutron g-factor, $r_c = e^2/m_e c^2 = 2.8\,\mathrm{fm}$ is the classical electron radius with e, m_e, and c the elementary charge, the electron mass, and the speed of light, respectively, $f(Q)$ is the atomic form factor of Co [50], $\mathbf{Q}$ is the scattering vector, and $\hat{\mathbf{Q}} = \mathbf{Q}/|\mathbf{Q}|$. We compute the correlation function from the spatiotemporal dynamics of our large spin cluster to all orders of the magnon-magnon interactions, without approximations [51]. We defer the details of the numerical procedure to the supplementary information [36].

In Fig. 4(a) and (b), we show the calculated spectra for the crystalline model and amorphous Co_4P at room temperature $T = 300$ K for $\mathbf{Q} \parallel [001]$. The excitations of the crystalline system are a periodic function of momentum transfer in the extended Brillouin zone scheme, with an amplitude that decays only weakly by the Co form factor. We observe a single magnon band, as expected for one spin per primitive unit cell.

We extract the spin wave stiffness D from our spectra by a fit to $\epsilon(Q) = DQ^2$, for $Q < 0.6$ Å^{-1}. In the FCC model [Fig. 4(a)] the stiffness is $D_{Co} = 182\,\mathrm{meV\,Å^2}$, whereas in the amorphous Co_4P model [Fig. 4(b)] the spin waves are softer with $D_{Co_4P} = 129\,\mathrm{meV\,Å^2}$, very close to the experimental results [11]. In crystalline magnets the magnon linewidth scales as $\sim \alpha\omega$, while the peaks are much broader in the amorphous material, as expected in disordered systems. At high energies, $\epsilon > 50$ meV, the spectrum becomes diffuse, i.e. well-defined magnon excitations cease to exist. In Fig. 4(b), we compare the numerical results with Eq. (1) in the QCA, which agrees quite well close to the origin and appears to model the modulation of the diffuse background at high energies.

At larger scattering vectors the amorphous magnetic spectrum shows a clear feature with parabolic dispersion and zero gap, centred at $Q \approx 3.1$ Å^{-1}, close to the observation [see Fig. 4(b)] and the first peak in the static structure factors (see Fig. 2). The calculated line width is close to that at the origin, indicating a coherent rather than diffuse magnon. The second minimum agrees with the reciprocal lattice vector of the FCC lattice with the same momentum density, which is the starting configuration of the Monte-Carlo procedure. We observe analogous minima at the Brillouin zone boundary in other crystal directions as well such as $\mathbf{Q} \parallel [111]$ (not shown). However, in contrast to the crystalline system of the artificial FCC Co where the spectrum repeats due to Bloch's theorem, these dips do not re-appear in the amorphous spectrum at higher values of Q. These minima are therefore caused by umklapp scattering from residual structural order, as suggested previously [29]. But we cannot confirm that these lead to a finite gap that is crucial for an exotic roton feature.

Conclusion. – Our calculations of the spin wave spectrum of amorphous Co_4P find a replica of the dispersion around the Γ-point, looks surprisingly similar to that of crystalline ferromagnets at low energies. This feature is similar to the so-called 'roton-like' local minimum but turns out to be gapless. We attribute it to umklapp scattering caused by residual local order and not by a complex magnetic texture such as a roton. The wavenumbers correspond to the first peak positions of observed structure factors. The sharp low frequency feature implies a contribution that is coherently periodic over many lattice constants in the magnon wave functions. In other words, the resulting amorphous structure retains some ordering. We note that in the original neutron scattering experiments [12], there is a comment that the peaks in the static structure factors were sharper than usually seen in amorphous materials, hinting at the possibility that these samples also retained some short range order. At high energies, the spectrum features no coherent magnons but a significant diffuse background that is caused by the alloy disorder [52, 53]. We note that the residual order which causes the umklapp scattering could be a more general phenomenon, even in glassy materials, which have similar static structure factors. We hope that our work will inspire renewed experimental efforts to measure magnons in amorphous materials that can test our predictions. If the gap is absent, we have a powerful method at hand to characterise the degree of disorder in non-ideal amorphous magnets. Our spin correlation functions are also an input for calculating spin transport properties in amorphous magnets via the Kubo formula [54].

We would like to thank K. Sato, K. Kobayashi, Y. Araki, and Y. Kawaguchi for valuable discussions. This work was supported by the Graduate Program in Spintronics (GP-Spin) at Tohoku University. Calculations were performed on ARC4, part of the High Performance Computing facilities at the University of Leeds. G. E. W. B. was supported by JSPS KAKENHI (19H00645). J. B. acknowledges support from the Royal Society through a University Research Fellowship. M. K. was supported by Grant-in-Aid for JSPS Fellows (JP19J20118) and GP-Spin at Tohoku University.

[1] W. H. Meiklejohn, "Magnetooptics: A thermomagnetic recording technology," Proc. IEEE **74**, 1570–1581 (1986).
[2] Stuart S. P. Parkin, Christian Kaiser, Alex Panchula, Philip M. Rice, Brian Hughes, Mahesh Samant, and See-Hun Yang, "Giant tunnelling magnetoresistance at room temperature with MgO (100) tunnel barriers," Nat. Mater. **3**, 862–867 (2004).
[3] S. U. Jen, Y. D. Yao, Y. T. Chen, J. M. Wu, C. C. Lee, T. L. Tsai, and Y. C. Chang, "Magnetic and electrical properties of amorphous CoFeB films," J. Appl. Phys. **99**, 053701 (2006).
[4] J. Barker, U. Atxitia, T. A. Ostler, O. Hovorka, O. Chubykalo-Fesenko, and R. W. Chantrell, "Two-magnon bound state causes ultrafast thermally induced magnetisation switching," Sci. Rep. **3**, 3262 (2013).
[5] Devin Wesenberg, Tao Liu, Davor Balzar, Mingzhong Wu, and Barry L. Zink, "Long-distance spin transport in a disordered magnetic insulator," Nat. Phys. **13**, 987–993 (2017).
[6] Héctor Ochoa, Ricardo Zarzuela, and Yaroslav Tserkovnyak, "Spin hydrodynamics in amorphous magnets," Phys. Rev. B **98**, 054424 (2018).
[7] Juan M. Gomez-Perez, Koichi Oyanagi, Reimei Yahiro, Rafael Ramos, Luis E. Hueso, Eiji Saitoh, and Fèlix Casanova, "Absence of evidence of spin transport through amorphous $Y_3Fe_5O_{12}$," Appl. Phys. Lett. **116**, 032401 (2020).
[8] Liupeng Yang, Yaoyu Gu, Lina Chen, Kaiyuan Zhou, Qingwei Fu, Wenqiang Wang, Liyuan Li, Chunjie Yan, Haotian Li, Like Liang, Zishuang Li, Yong Pu, Youwei Du, and Ronghua Liu, "Absence of spin transport in amorphous YIG evidenced by nonlocal spin transport experiments," Phys. Rev. B **104**, 144415 (2021).
[9] J. M. D. Coey, "Amorphous magnetic order," J. Appl. Phys. **49**, 1646–1652 (1978).
[10] R. C. O'Handley, "Physics of ferromagnetic amorphous alloys," J. Appl. Phys. **62**, R15–R49 (1987).
[11] T. Kaneyoshi, *Amorphous Magnetism* (CRC-Press, 1984).
[12] H. A. Mook, N. Wakabayashi, and D. Pan, "Magnetic Excitations in the Amorphous Ferromagnet Co_4P," Phys. Rev. Lett. **34**, 1029–1033 (1975).
[13] R. P. Feynman, "Atomic Theory of Liquid Helium Near Absolute Zero," Phys. Rev. **91**, 1301–1308 (1953).
[14] R. P. Feynman and Michael Cohen, "Energy Spectrum of the Excitations in Liquid Helium," Phys. Rev. **102**, 1189–1204 (1956).
[15] Weihong Zheng, John O. Fjærestad, Rajiv R. P. Singh, Ross H. McKenzie, and Radu Coldea, "Anomalous excitation spectra of frustrated quantum antiferromagnets," Phys. Rev. Lett. **96**, 057201 (2006).
[16] Weihong Zheng, John O. Fjærestad, Rajiv R. P. Singh, Ross H. McKenzie, and Radu Coldea, "Excitation spectra of the spin-$\frac{1}{2}$ triangular-lattice heisenberg antiferromagnet," Phys. Rev. B **74**, 224420 (2006).
[17] Oleg A. Starykh, Andrey V. Chubukov, and Alexander G. Abanov, "Flat spin-wave dispersion in a triangular antiferromagnet," Phys. Rev. B **74**, 180403(R) (2006).
[18] Jason Alicea, Olexei I. Motrunich, and Matthew P. A. Fisher, "Theory of the algebraic vortex liquid in an anisotropic spin-$\frac{1}{2}$ triangular antiferromagnet," Phys. Rev. B **73**, 174430 (2006).
[19] Jason Alicea and Matthew P. A. Fisher, "Critical spin liquid at $\frac{1}{3}$ magnetization in a spin-$\frac{1}{2}$ triangular antiferromagnet," Phys. Rev. B **75**, 144411 (2007).
[20] Takahito Kaneyoshi, "Spin Waves in Amorphous Ferromagnets," J. Phys. Soc. Jpn. **45**, 1835–1841 (1978).
[21] Laura M. Roth, "Analysis of effective-medium approximation for a tight-binding model of a liquid metal," Phys. Rev. B **11**, 3769–3779 (1975).
[22] L. M. Roth and V. A. Singh, "Comment on spin wave excitations in amorphous ferromagnets," Phys. Lett. A **59**, 49–51 (1976).
[23] Vijay A. Singh and L. M. Roth, "Spin waves in amorphous ferromagnets," J. Appl. Phys. **49**, 1642–1644 (1978).
[24] R. Alben, "Spin waves in a model for an amorphous ferromagnet," AIP Conf. Proc. **29**, 136–140 (1976).
[25] G. David Scott, "Radial Distribution of the Random Close Packing of Equal Spheres," Nature **194**, 956–957 (1962).
[26] G. S. Cargill, "Dense Random Packing of Hard Spheres as a Structural Model for Noncrystalline Metallic Solids," J. Appl. Phys. **41**, 2248–2250 (1970).
[27] P. H. Gaskell, "On the structure of simple inorganic amorphous solids," J. Phys. C: Solid State Phys. **12**, 4337–4368 (1979).
[28] John L. Finney, "Bernal's road to random packing and the struc-

ture of liquids," Philos. Mag. **93**, 3940–3969 (2013).
[29] G. Shirane, J. D. Axe, C. F. Majkrzak, and T. Mizoguchi, "Magnetic excitations in amorphous ferromagnets," Phys. Rev. B **26**, 2575–2583 (1982).
[30] H. A. Mook and C. C. Tsuei, "Magnetic excitations in amorphous $Fe_{75}P_{15}C_{10}$," Phys. Rev. B **16**, 2184–2190 (1977).
[31] R. L. McGreevy, "Reverse Monte Carlo modelling," J. Phys.: Condens. Matter **13**, R877–R913 (2001).
[32] O. Gereben, P. Jóvári, L. Temleitner, and L. Pusztai, "A new version of the RMC++ Reverse Monte Carlo programme, aimed at investigating the structure of covalent glasses," J. Optoelectron. Adv. Mater. **9**, 3021–3027 (2007).
[33] J. F. Sadoc and J. Dixmier, "Structural investigation of amorphous CoP and NiP alloys by combined X-ray and neutron scattering," Mater. Sci. Eng. **23**, 187–192 (1976).
[34] In the RMC++ manual (version 1.4) n_Q is not included in the equation, but the cost function is in fact normalised.
[35] Orsolya Gereben, *RMC_ POT user guide for version 1.4* (2015).
[36] See Supplemental Material at [URL will be inserted by publisher] for additional details of the RMC procedure and numerical implementations within the spin dynamics.
[37] B. L. Gyorffy, A. J. Pindor, J. Staunton, G. M. Stocks, and H. Winter, "A first-principles theory of ferromagnetic phase transitions in metals," J. Phys. F: Met. Phys. **15**, 1337–1386 (1985).
[38] B. Skubic, J. Hellsvik, L. Nordström, and O. Eriksson, "A method for atomistic spin dynamics simulations: implementation and examples," J. Phys.: Condens. Matter **20**, 315203 (2008).
[39] C. H. Woo, Haohua Wen, A. A. Semenov, S. L. Dudarev, and Pui-Wai Ma, "Quantum heat bath for spin-lattice dynamics," Phys. Rev. B **91**, 104306 (2015).
[40] J. Durand and M. F. Lapierre, "NMR of Co_{59} in amorphous CoP alloys," J. Phys. F: Met. Phys. **6**, 1185–1192 (1976).
[41] Joseph Barker and Gerrit E. W. Bauer, "Semiquantum thermodynamics of complex ferrimagnets," Phys. Rev. B **100**, 140401(R) (2019).
[42] Naohiro Ito, Takashi Kikkawa, Joseph Barker, Daichi Hirobe, Yuki Shiomi, and Eiji Saitoh, "Spin Seebeck effect in the layered ferromagnetic insulators $CrSiTe_3$ and $CrGeTe_3$," Phys. Rev. B **100**, 060402(R) (2019).
[43] Joseph Barker, Dimitar Pashov, and Jerome Jackson, "Electronic structure and finite temperature magnetism of yttrium iron garnet," Electron. Struct. **2**, 044002 (2020).
[44] G. S. Cargill and R. W. Cochrane, "AMORPHOUS COBALT-PHOSPHORUS ALLOYS : ATOMIC ARRANGEMENTS AND MAGNETIC PROPERTIES," J. Phys. Colloques **35**, C4–269–C4–278 (1974).
[45] R. W. Cochrane and G. S. Cargill, "Magnetization of Amorphous CoP Alloy—Spin Waves in Noncrystalline Ferromagnets," Phys. Rev. Lett. **32**, 476–478 (1974).
[46] M. A. Continentino and N. Rivier, "On the apparent spin wave stiffness of amorphous ferromagnets," J. Phys. F: Met. Phys. **9**, L145–L150 (1979).
[47] J. D. Axe, L. Passell, and C. C. Tsuei, "Spin waves in an amorphous metallic ferromagnet," AIP Conf. Proc. **24**, 119–120 (1975).
[48] J. D. Axe, G. Shirane, T. Mizoguchi, and K. Yamauchi, "Neutron scattering study of spin waves in the amorphous metallic ferromagnet $(Fe_{93}Mo_7)_{80}B_{10}P_{10}$," Phys. Rev. B **15**, 2763–2770 (1977).
[49] W. Marshall and S. W. Lovesey, *Theory of Thermal Neutron Scattering: The Use of Neutrons for the Investigation of Condensed Matter* (Oxford University Press, 1971).
[50] E. Price, ed., "International Tables for Crystallography Vol. C," (International Union of Crystallography, 2006) Chap. 4.4, pp. 430–487.
[51] W. Marshall and R. D. Lowde, "Magnetic correlations and neutron scattering," Rep. Prog. Phys. **31**, 705–775 (1968).
[52] J. F. Sadoc, J. Dixmier, and A. Guinier, "Theoretical calculation of dense random packings of equal and non-equal sized hard spheres applications to amorphous metallic alloys," J. Non-Cryst. Solids **12**, 46–60 (1973).
[53] T. Fukunaga, K. Itoh, T. Otomo, K. Mori, M. Sugiyama, H. Kato, M. Hasegawa, A. Hirata, Y. Hirotsu, and A.C. Hannon, "Voronoi analysis of the structure of Cu–Zr and Ni–Zr metallic glasses," Intermetallics **14**, 893–897 (2006).
[54] Alexander Mook, Börge Göbel, Jürgen Henk, and Ingrid Mertig, "Magnon transport in noncollinear spin textures: Anisotropies and topological magnon hall effects," Phys. Rev. B **95**, 020401(R) (2017).